Article:

Yuan, R, Yu, HS orcid.org/0000-0003-3330-1531, Yang, DS et al. (1 more author) (2019) On a fabric evolution law incorporating the effects of b-value. Computers and Geotechnics, 105. pp. 142-154. ISSN 0266-352X

https://doi.org/10.1016/j.compgeo.2018.09.019

On a fabric evolution law incorporating the effects of b-value

Dr Ran Yuan

Key Laboratory of High-speed Railway Engineering (Southwest Jiaotong University), Ministry of Education

Email: yuanran@swjtu.edu.cn

Professor Hai-Sui YU

School of Civil Engineering,

University of Leeds, Leeds LS2 9JT, UK

Email: h.yu@leeds.ac.uk

Dr Dun-Shun Yang

Nottingham Centre for Geomechanics,

University of Nottingham, Nottingham NG7 2RD, UK

Email: dunshun.yang@arup.com

Dr Nian Hu

Corresponding author

Nottingham Centre for Geomechanics,

University of Nottingham, Nottingham NG7 2RD, UK

Email: greaterhu@163.com

ABSTRACT

In this paper, the effects of the intermediate stress ratio, i.e., b-value ($b=(\sigma_2-\sigma_3)/(\sigma_1-\sigma_3)$), on the contact normal-based fabric evolution of granular material, are incorporated into an extant hybrid fabric evolution law. The new evolution law is validated by Discrete Element Method (DEM) simulation results under monotonic shearing with different b-values. Predictions of the proposed generalized fabric evolution law agree well with the DEM simulation results. This evolution law can be widely used for constitutive modelling of granular materials, considering the effects of b-value in a general geomechanical three-dimensional stress space.

Keywords: Fabric evolution; Evolution law; Effects of b-value; DEM

1 Introduction

Most field problems in geotechnical engineering, e.g., earthquake, traffic loading, and river embankments, involve a general loading condition ($\sigma_1 \geq \sigma_2 \geq \sigma_3$), where soils are subject to complicated loading paths, together with changes in the magnitudes of the three principal stresses (i.e., σ_1, σ_2 and σ_3) and rotations of their directions. Real soils, especially sands, are loading path dependent. This means that their behaviours are affected by the magnitudes of the three principal stresses and their directions; hence, it is significant to take all the three principal stresses into consideration in geotechnical engineering design and construction.

One interesting aspect of soil response is the sensitivity of the mechanical soil behaviour to the intermediate stress ratio, i.e., b-value. The b-value is introduced as a non-dimensional parameter $b=(\sigma_2-\sigma_3)/(\sigma_1-\sigma_3)$, where σ_1 and σ_3 are the major and minor principal stresses, respectively. The b-value is widely used to describe the effects of intermediate principal stress (σ_2), which was first proposed by Habib [1], who performed a series of torsional triaxial tests to investigate the strength characteristics of clays and sands. Bishop [2] determined that the influence of intermediate principal stress σ_2 on soil response can be more readily appreciated in terms of b-value rather than σ_2 itself. In the early 1960s, a number of researchers focused on the study of the effects of the b-value on the soil behaviours, e.g., Bjerrum and Kummeneje [3] and Cornforth [4]. A review of the above work was made by Oda et al [5], who compared triaxial and plane-strain test results and noted that (1) the friction angle in plane strain testing (b=0.2~0.3) is up to 10% ~ 20% larger than that in triaxial compression testing (b=1.0) for dense sand tested under a low confining pressure and (2) the strain to failure is smaller in plane strain testing (b=0.2~0.3) than that in triaxial compression testing (b=1.0) for sands of similar densities. It is obvious, from their observations, that the b-value demonstrates significant effects on soil strength and stress-strain behaviours. Similar findings in the experiments were proposed by using various advanced testing apparatuses, e.g., triaxial testing [6-8] and Hollow cylinder testing [9-12]. Recently, DEM simulations have been used to perform cubic triaxial testing (e.g., [13, 14]) and Hollow cylinder testing (e.g., [15, 16]) and demonstrated good consistency with experimental behaviours. These findings in both the laboratory and DEM simulations confirmed and enhanced the conclusions that b-value has significant effects on the deformation and strength behaviour of granular materials, e.g., sands.

From micromechanical analysis [17, 18], the effects of b-value on strength are strongly linked to the distribution of the contact normal, hence to the fabric tensor based on the contact normal [19, 20]. For example, the stress-force-fabric relationship suggests that the peak stress ratio is dependent on the contact normal distribution anisotropy [21, 22]. Evidence from DEM simulations has directly demonstrated that peak fabric anisotropy [13, 23] and critical fabric anisotropy [24] are not circular in the deviatoric plane for different b-values. These effects are also confirmed by the DEM simulations carried out by Li et al [15].

Several formulations have been proposed to characterize the effects of b-value on the peak and residual strengths of both the initial isotropic and anisotropic granular materials [25-29]. These formulations for constitutive modelling are developed phenomenologically. Indeed, phenomenological models have shown their abilities to capture the macro effects of b-value, the evolution of the internal structure however is ignored in phenomenological models. In addition, those models introduced too many parameters without physical meanings and are difficult for calibration. On the other hand, an increasing interest in microscopic modelling and multi-scale approaches is rising, e.g., fabric-based constitutive modelling. Fabric evolution law, accounting for the microscopic information, is the essential element to develop fabric-based constitutive models for anisotropic behaviours of granular materials. To develop constitutive models considering the effects of b-value as well as anisotropy, the effects of b-value on the fabric evolution law should be considered. Since the sensitivity of the b-value on the mechanical response of the granular materials has been widely identified, many researcher (e.g., [30, 31]) have tried to incorporate this feature into their three dimensional constitute models. However, the effects of the b-value on the fabric evolution, e.g. the critical stress ratio and the critical fabric anisotropy (as evident above), has not been displayed yet.

In this paper, we generalize a hybrid fabric evolution law, which is calibrated with results of fabric evolution statistically obtained from the micro-scale geometrical quantities, to incorporate the effects of b-value on the evolution of fabric. To achieve this, we incorporate the effects of b-value into the proposed hybrid evolution law by assuming that C_1 and C_F are dependent on the b-value in terms of the Lode angle θ_l. The modified evolution law considers both the effects of anisotropy and b-value on the fabric evolution. It can be widely used for fabric-based constitutive modelling of granular materials responding to general stress paths, together with simple isotropic constitutive models, such as the Cam clay Model, Modified Cam clay Model, or the Clay and Sand Model (CASM) proposed by Yu [32, 33]. However, this work is beyond the scope of this paper and will be presented in a future paper.

2 Generalization of the fabric evolution law

2.1 Definitions of fabric tensor

As shown in Fig. 1, for each contact point, there are two types of unit contact normal, $\boldsymbol{n}$ and $-\boldsymbol{n}$.

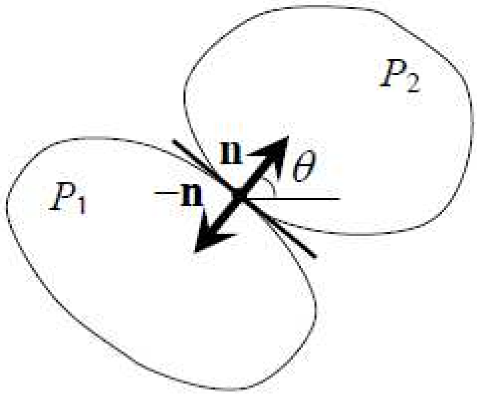

Fig.1 Definition of the contact normal

The relative frequency distribution of the contact normal may be described by a probability density function $\boldsymbol{E}(\boldsymbol{n})$.The density function is defined so that it satisfies the following equation:

$$\int_{\Omega} E(\boldsymbol{n}) d\Omega = 1 \tag{1.1}$$

where $\Omega = \frac{A}{r^2}$ is a solid angle for the three dimensional space; A denotes the spherical surface area and r denotes the radius of the considered sphere. Given that each point has two types of contact normal opposite to each other, we must have:

$$E(\boldsymbol{n}) = E(-\boldsymbol{n}) \tag{1.2}$$

In most cases in three dimensional materials (e.g., [21-22, 35-36]), it can be truncated by spherical harmonic series in second-order as

$$E(\boldsymbol{n}) = \frac{1}{4\pi}(1 + \boldsymbol{F}: \boldsymbol{n} \otimes \boldsymbol{n}) \tag{1.3}$$

The tensor $\boldsymbol{F}$ in equation (1.3) is known as the second-order fabric tensor of the third kind in terms of unit contact normal. Fabric tensor $\boldsymbol{F}$ is traceless, and can be used to describe the fabric anisotropy in the assembly.

Practically, the tensor $\boldsymbol{F}$ can be estimated from the second-order fabric tensor $\boldsymbol{N}$ as follows (e.g, [21, 34, 36-37]):

$$\boldsymbol{F} = \frac{15}{2}\left(\boldsymbol{N} - \frac{1}{3}\boldsymbol{I}\right) \tag{1.4}$$

where $\boldsymbol{N}$ can be determined from the discrete directional contact normal $\boldsymbol{n}$ of a granular assembly by

$$\boldsymbol{N} = \frac{1}{N_c}\sum_{c\in N_c}\boldsymbol{n}^c \otimes \boldsymbol{n}^c \tag{1.5}$$

2.2 Fabric tensor at a critical state

Granular materials under monotonic shearing will achieve a critical state characterised by stationary values of stress, void ratio with the unlimited development of shear strain [38-41]. We redefine the anisotropic fabric state by adding one more equation which enables a requirement on fabric tensor at the critical state (critical fabric tensor) into the conventional definition of the critical state. The critical fabric tensor $\boldsymbol{F}_c$ is assumed to be proportional with the deviatoric stress ratio tensor $\boldsymbol{\eta}$ at the critical state, i.e.

$$\boldsymbol{F}_c = C_F(b)\boldsymbol{\eta}_c = C_F(b)\left(\frac{\boldsymbol{S}}{p}\right)_c \tag{1.6}$$

where C_F is a proportional coefficient generally dependent on the b-value, $\eta_c = \sqrt{3/2}\,\|\boldsymbol{\eta}\|$, s is the stress deviator and p is the mean effective stress.

The spatial distribution of contact normal keeps evolving to support the mobilised strength. The rate of the fabric, i.e., $\dot{\boldsymbol{F}}$, is characterized by the fabric evolution law; hence the physical description of the rate of the fabric is defined as the changing of the spatial distribution of contact normal. In this paper, a hybrid fabric evolution law has been proposed based on the principle of material frame indifference, with the assumption of rate-independency and unique critical fabric state, i.e.,

$$\dot{\boldsymbol{F}} = C_1(1 + C_2\|\boldsymbol{\eta}\|)\dot{\boldsymbol{\eta}} + C_3\dot{\Lambda}(C_F\boldsymbol{\eta} - \boldsymbol{F}) \tag{2.1}$$

$$C_F = \left(\frac{F_q}{\eta}\right)_c, F_q = \sqrt{3/2}\,\|\boldsymbol{F}\|, \eta = \sqrt{3/2}\,\|\boldsymbol{\eta}\| \tag{2.2}$$

where C_1, C_2, C_3 are material constants controlling the rate of fabric tensor, hence the microscopic mechanisms of the fabric evolution; $\boldsymbol{\eta} = \boldsymbol{S}/p$ is a stress ratio tensor representing the deviatoric stress tensor $\boldsymbol{S}$ normalized by the mean stress p; $\dot{\Lambda}$ is a norm of rate of the deviatoric plastic strain, i.e., $\dot{\Lambda} = \|\dot{e_p}\|$; F_q determines the fabric deviator.

It is postulated in the evolution law that the rate of the fabric tensor, which is defined on the contact normal, is related to both the rate of the stress ratio tensor and the plastic strain rate tensor, respectively reflect two different microscopic mechanisms of the fabric evolution. At the initial stage of shearing, as the rapid increase of the stress ratio, contacts are forced to reorganize to support the applied stress. The change of distribution of contact normal, hence the evolution of fabric tensor, is mainly due to the net creation of the contacts, and thus is dominated by the stress ratio rate. This is characterized as the first microscopic mechanisms of the fabric evolution, which is controlled by C_1 and C_2. At a large shear strain, the net rate of contact creation decreases considerably, and the change of contact normal distribution is controlled by the migration of contact point through sliding and rolling of particles across each other, which can be assumed to be related to the plastic strain rate. This is characterized as the second microscopic mechanisms of the fabric evolution, which is controlled by C_3.

This evolution law captures the fabric evolution law in the entire stress ratio range and all loading directions under a monotonic loading. These findings have been validated with a satisfactory agreement by monotonic DEM simulations. Details of the validation can be found in Hu [42]. However, the effects of b-value have not been fully considered in this evolution law, which will be shown as follows.

2.1 Influence of b-value on the critical stress ratio

From equation (2.2), we see that C_F is dependent on the critical stress ratio and the critical fabric anisotropy. It is well known that the critical stress ratio $M = \eta_c$ is dependent on b-value or Lode angle θ_l. The following equation [28, 33] is used to characterize the relationship between M and Lode angle θ_l:

$$M(\theta) = M_{cc}h_1(\theta), h_1(\theta) = \left(\frac{2{l_1}^4}{1+{l_1}^4+\left(1-{l_1}^4\right)sin(3\theta_l)}\right)^{1/4}, l_1 = \frac{M_{ct}}{M_{cc}} \quad (3.1)$$

where M_{ct} and M_{cc} are the critical stress ratios for triaxial compression and extension. If we assume that the frictional angles on the shear plane for both extension and compression are the same, it can be estimated that

$$M_{cc} = \frac{6\sin(\phi_{cv})}{3-\sin(\phi_{cv})}, M_{ct} = \frac{6\sin(\phi_{cv})}{3+\sin(\phi_{cv})}, \sin(\phi_{cv}) = \left(\frac{\sigma_1-\sigma_3}{\sigma_1+\sigma_3}\right)_c \tag{3.2}$$

where ϕ_{cv} is the critical frictional angle. According to relationships in equation (3.2), l_1 can be expressed in terms of M_{cc} as

$$l_1 = \frac{3}{3+M_{cc}} \tag{3.3}$$

In equation (3.1), function $h_1(\theta_l)$ determines the shape of M in the π plane (see Fig. 2). For triaxial compression loading paths, $\theta_l = -\pi/6, h_1(\theta_l) = 1, M = M_{cc}$; for triaxial extension loading paths, $\theta_l = \pi/6, h_1(\theta) = l_1, M = M_{ct}$. This relationship was proven to be realistic when compared with experimental data. One merit of this shape function is that it is convex for a larger range of choices of l_1 [43]. We also use equation (3) to predict the critical stress ratios for various lode angles from the DEM triaxial compression results obtained by Zhao and Guo [24].The comparison between predictions obtained by the relationship in equation (3) with the DEM simulation results is shown in Fig. 2. Note that the results have been normalized by $M_{cc} = 0.6\sqrt{3/2}$, and that l_1 is obtained by equation (3.3). It can be seen in Fig. 2 that equation (3) with l_1 estimated by equation (3.3) can capture the critical stress ratio for different b-values well.

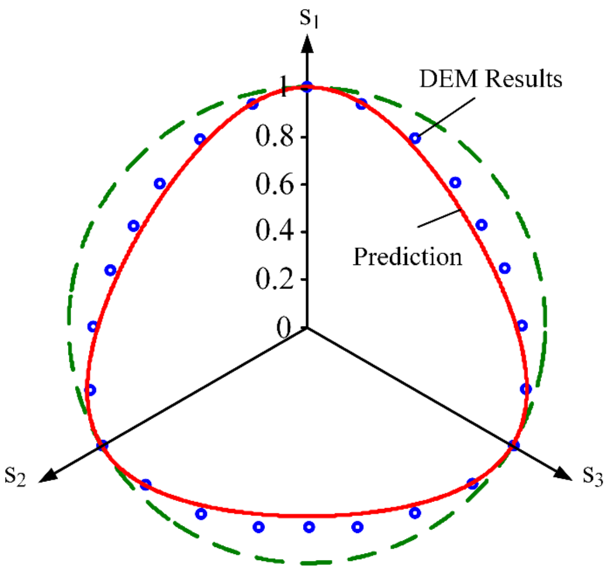

Fig. 2 Theoretical predictions and DEM results of critical stress ratios in the π plane

2.2 Influence of b-value on the critical fabric anisotropy

From the DEM tests results [24] in Fig. 3, it can be seen that the shape function for the critical fabric ratio $M_F = F_{qc}$ is not a circle in the π plane, which means that M_F is also dependent on the Lode angle. A similar shape function to equation (3.1) is observed. However, M_F under triaxial extension is greater than that under triaxial compression, which is different from the case for a critical stress ratio. The differences imply that the shape parameter l_2 for critical fabric anisotropy should be different from the shape parameter l_1 for the critical stress ratio. The critical fabric ratio M_F is assumed to be a function of Lode angle as

$$M_F(\theta_l) = M_{Fc} h_2(\theta_l), h_2(\theta_l) = \left(\frac{2{l_2}^4}{1+{l_2}^4+(1-{l_2}^4)sin(3\theta_l)}\right)^{1/4}, l_2 = \frac{M_{Ft}}{M_{Fc}} \qquad (4)$$

where M_{Ft} and M_{Fc} are the critical fabric ratios for triaxial compression and extension shearing, respectively. In equation (4), $h_2(-\pi/6) = 1, M_F = M_{Fc}; h_2(\pi/6) = 1, M_F = M_{Ft}$. An empirical equation based on the DEM test results carried out by Zhao and Guo [24] suggests that

$$l_2 = 1/l_1 \tag{5}$$

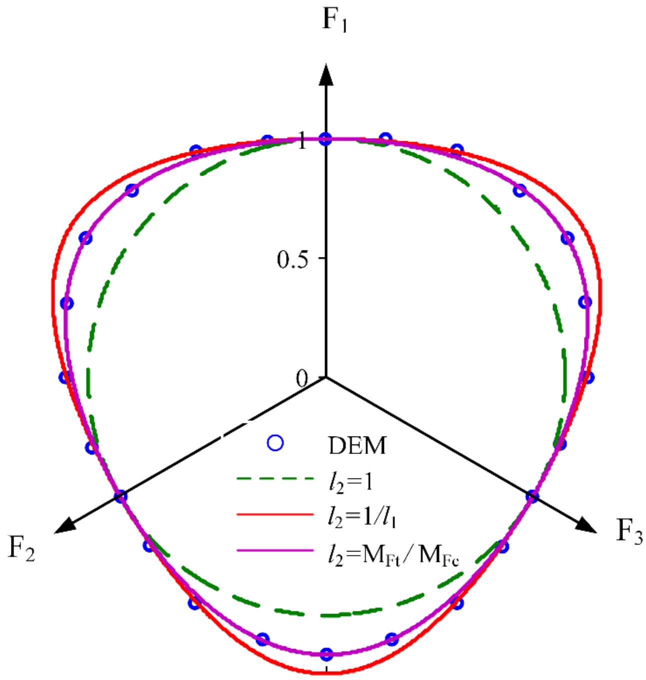

Fig. 3 Theoretical predictions and DEM results of critical fabric ratios in the deviatoric plane

In general, we can choose l_1 and l_2 independently. If M_{F_t}/M_{F_c} is not available, then we can use equation (5) to estimate l_2 instead. Fig. 3 presents the comparison between the predictions from the relationship in equation (4) with different choices of shape parameter l_2 and the DEM results by Zhao and Guo [24], in which the fabric deviator $M_F(\theta_l)$ has been normalized by M_{Fc}. It can be seen that the prediction of equation (4) perfectly agrees with the DEM results. The estimation of l_2 by equation (5) leads to an acceptable gap between the DEM results and the theoretical prediction.

2.3 The generalized fabric evolution law

The dependency of $M_F(\theta_l)$ and $M(\theta_l)$ on different shape parameters makes C_F dependent on the Lode angle. The second term on the right side of the evolution law in equation (2.1) represents the second evolution mechanism related to the plastic strain rate. The dependency of C_F on the Lode angle introduces the effect of b-value on the second evolution law mechanism. The first term on the right side of the evolution law in equation (2.1) represents the first fabric evolution mechanism related to the rate of stress ratio increment and dominates before reaching the peak stress ratio. To consider the effects of b-value on the first fabric evolution mechanism, C_1 is assumed to be dependent on the Lode angle and is replaced by $C_1 h_3(\theta_l)$ with a new shape parameter l_3. The shape function $h_3(\theta_l)$ is written as

$$h_3(\theta) = \left(\frac{2{l_3}^4}{1+{l_3}^4+(1-{l_3}^4)sin(3\theta_l)}\right)^{1/4}, \quad l_3 = 1/l_1 \tag{6}$$

This estimation is proposed based on the observation from the DEM results from Thornton [13, 23]. Thornton presents the response of fabric anisotropy in the π plane for different b-values at different shearing strain before softening. Compared with the critical fabric anisotropy in Fig. 4, the shape function of the fabric response in the π plane is quite similar at different levels of the shear strain. The estimation of $l_3 = 1/l_1$ is assumed with the consideration of avoiding too many material parameters. The consequence of this estimation will be illustrated in details in section 3.2.

A new evolution law considering the effect of b-value is generalized from the hybrid evolution law in equation (2) as:

$$\dot{\boldsymbol{F}} = C_1 h_3(\theta_l)(1 + C_2\|\boldsymbol{\eta}\|)\dot{\boldsymbol{\eta}} + C_3\dot{\Lambda}(C_F(\theta_l)\boldsymbol{\eta} - \boldsymbol{F}), C_F(\theta_l) = \frac{M_F(\theta_l)}{M(\theta_l)} \tag{7}$$

In this evolution law, the function $C_F(\theta_l)$ considers the effects of b-value on the second evolution mechanism, while the function $h_3(\theta_l)$ considers the effects of b-value on the first evolution mechanism. As both function $C_F(\theta_l)$ and $h_3(\theta_l)$ are functions of stress invariants of the stress tensor, the evolution law satisfies the requirement of the principle of material-frame indifference. The attractor '$C_F(\theta_l)\boldsymbol{\eta} - \boldsymbol{F}$' ensures that the new evolution law reaches a unique critical fabric, which is proportional to the stress ratio tensor $\boldsymbol{\eta_c}$, under monotonic shearing.

When we choose the shape parameters as $l_2 = l_1, l_3 = 1$, the evolution law in equation (7) reduces to the evolution law in equation (2).

3 Validation of the generalised evolution law

A series of DEM simulations, by using the PFC^{3D} software ([44]), are performed to validate the generalised evolution law. The behaviour at contacts is modelled by a soft-contact approach, which allows vanishing small overlapping between rigid particles. The linear contact model, i.e., the Hookean model is used to describe the local contact behaviour. The ratio between the tangential and normal stiffness can provide the Poisson's ratio. In order to minimize possible boundary arching effects, a convex polyhedral (polygonal) shape of the specimen is used, and a set of massless infinite rigid walls are specified to form a polyhedral-shaped boundary (e.g., Fig.4). The specimen size is chosen to be relatively larger compared with the particle size to accommodate around 11090 and 10151 particles for dense and loose specimens, respectively.

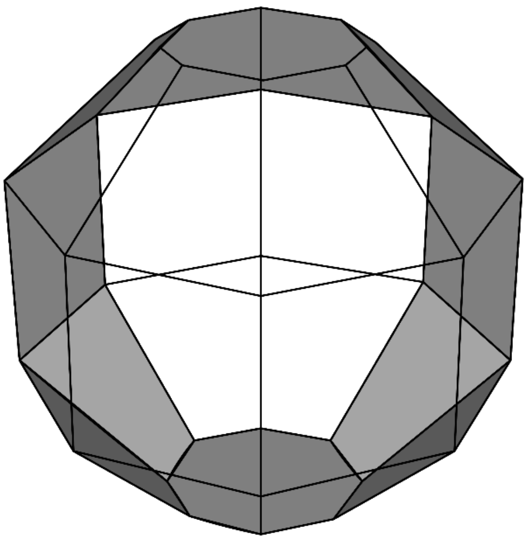

Fig.4 Example of polyhedron, n=8

The main mechanical behaviour of granular materials that we are interested in, e.g., the stress-strain relationship, volumetric strain, shear strain and soil anisotropy, can be reproduced satisfactorily by using spherical particles. The anisotropic packing structure of granular assembly with spherical particles is confirmed by experimental isotropic compression tests (e.g., [45-46]). Hence, the spherical particles are used in this study for the sake of simplicity.

A series of parametric studies have been done to determine a proper grain radius range, which can balance the number of particles and the computational efficiency. In addition, a larger range of grain radius may result in the fact that small particles enter into the voids between the larger particles. Hence in this study, the radius of spherical particles consisting of numerical sample is randomly distributed between the range of 0.3mm and 0.5mm.

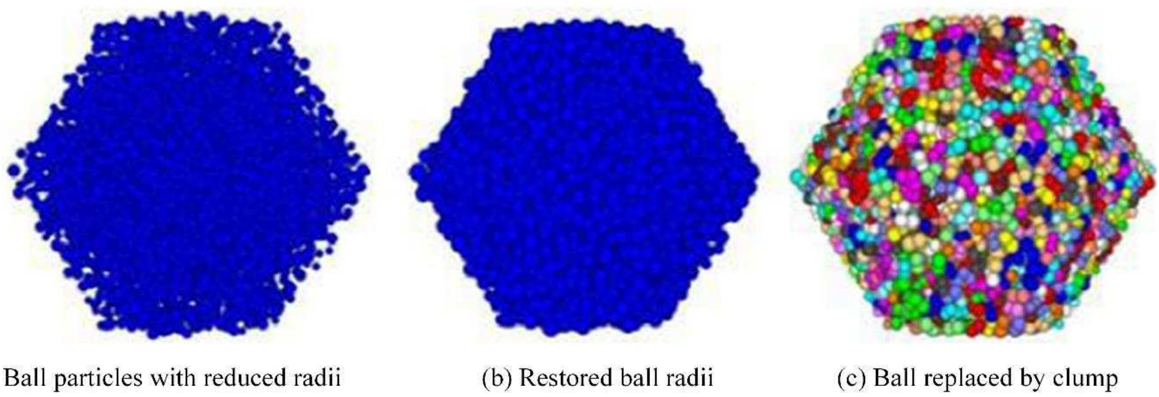

Fig. 5 Isotropic sample preparation by the radius expansion method

The sample of spherical particles is prepared by using the radius expansion method to generate initial isotropic sample with varying initial void ratios (Fig.5). The dense and loose samples with spherical particles are generated by specifying the frictional coefficients u_g=0.5 and u_g=0.1, respectively. Then the samples are isotropically consolidated to the confining pressure of p=500kPa. At this stage, the initial void ratios are 0.64 and 0.79, corresponding to dense and loose samples. Then the friction coefficient u is restored to the representative value u=0.5 and the samples are ready for simulations. The drained true triaxial loading path is applied, and the principal direction $\mathbf{n}^{\sigma}$ is unchanged while the deviatoric strain ε_q continuously increases. A mixed controlled boundary is employed with partially stress-controlled and partially strain-controlled, details can be referred to Li et al [15, 47]. During monotonic shearing for all tests, the mean pressure remains at 500 kPa with various b-values. The b-value ranges from 0 to 1 at an interval of 0.2. Since simulations of quasi-static granular material behaviour are focused, the mechanical damping is introduced to dissipate energy by damping particle motions. The local damping is employed. In the virtual experiments to be presented, the Cauchy stress and Biot strain definitions are followed [48]. The input parameters for the DEM simulation are listed in Table 1.

Table 1 DEM simulation properties

Number of particles	Dense specimen:11090 Loose specimen: 10151
Particle solid density ρ	2700 kg/m^3
Spherical particle radius r	[0.3,0.5] mm
Contact model	Linear stiffness
Normal stiffness for ball and wall	k_n=1×10^5 N/m
Tangential stiffness for ball and wall	k_s=1×10^5 N/m
Initial void ratio e_0	Dense specimen: 0.64 Loose specimen:0.79
Target loading path	True triaxial
Damping coefficient	x=0.7

The implicit Euler algorithm is used to integrate the evolution law. The evolution law in a rate form can be rewritten as

$$\boldsymbol{F}_{n+1} - \boldsymbol{F}_n = C_1 h_3(\theta_{n+1})(1 + C_2\|\boldsymbol{\eta}_{n+1}\|)(\boldsymbol{\eta}_{n+1} - \boldsymbol{\eta}_n) + C_3\dot{\Lambda}(C_F(\theta_{n+1})\boldsymbol{\eta}_{n+1} - \boldsymbol{F}_{n+1}) \quad (8.1)$$

where $\dot{\Lambda}$ is a discrete form of the norm of deviatoric plastic strain rate, i.e.

$$\dot{\Lambda} = \|\boldsymbol{e}_{n+1} - \boldsymbol{e}_n\| \quad (8.2)$$

We arrive at a sub load step n+1, as:

$$\boldsymbol{F}_{n+1} = \frac{C_1 h_3(\theta_{n+1})(1+C_2\|\boldsymbol{\eta}_{n+1}\|)(\boldsymbol{\eta}_{n+1}-\boldsymbol{\eta}_n)+\dot{\Lambda}C_3 C_F(\theta_{n+1})\boldsymbol{\eta}_{n+1}+\boldsymbol{F}_n}{1+C_3\dot{\Lambda}} \quad (8.3)$$

Then, given that the initial fabric tensor $\boldsymbol{F}_1 = \boldsymbol{F}_i$, stress ratios $\boldsymbol{\eta}_{n+1}, \boldsymbol{\eta}_n$ and deviatoric strains $\boldsymbol{e}_{n+1}, \boldsymbol{e}_n$, we adopt these stresses and strain paths obtained by DEM tests as the integration paths and calculate the fabric tensor using equation (8.2) for each sub-load step. The parameters used for theoretical predictions are listed in Table 2. The parameters M_{cc}, M_{Fc}, M_{Ft} can be obtained directly from the DEM simulation results directly. From these independent parameters, shape parameters can be obtained. From equation (3), $M_{ct} = 0.62; l_1 = 0.795$. The shape parameter l_2 is determined by the definition of $l_2 = M_{Ft}/M_{Fc}$. The shape parameter l_3 is estimated from equation (6). Parameters C_1,C_2, C_3, which control the rate of fabric tensor, cannot be determined directly. They are determined by the regressive analysis through the known stress, strain rate and fabric information obtained from DEM simulations. The effects of C_1,C_2, C_3 will be investigated through parametric analysis in section 3.2.

Table 2 Parameters of the generalised fabric evolution law

C_1	C_2	C_3	Mcc	M_{Fc}	M_{Ft}
0.1	6	7.6	0.78	0.66	0.77

3.1 Comparison with DEM simulation results

3.11 Comparison of the stress-strain and volumetric strain curve between DEM and experimental results

Fig.6 and Fig.7 illustrate the effects of b-value on the responses of stress-strain relationships and volumetric strain, respectively obtained from DEM simulations and experimental Hollow Cylinder Testing from Yang et al [12]. Here the dense specimen is taken as an example. It should be noted that Leighton Buzzard sand has been used by Yang et al [12], which is different from the samples that are used in our study. Hence, we only focus on the comparison of the trend other than the exact magnitude, between the DEM simulation results and experimental results. Regarding the effects of b-value on the stress strain curves as shown in Fig. 6 (a) and Fig.7, the trends of both curves obtained from the DEM simulations and laboratory testing, respectively are consistent. The stress ratio is decreasing with an increase in the b-value. Volumetric strains start to dilate at the beginning of shearing, and more dilative behaviour are observed at a greater b-value, for both DEM simulations and experimental findings (Fig.6 b and Fig.7). The only difference is that the variation of dilatancy is larger showing by the experimental results, when compared to the DEM simulation results. This difference may be attributed to the fact that shear band develops quickly for the hollow cylindrical sample; however, shear band is not considered in our DEM simulations.

Similar experimental investigations regarding effects of b-value on sand behaviours, in terms of the stress-strain and volumetric strain, have been reported for dense samples in the literature (e.g., [6, 49]). The investigations regarding the loose samples can be referred to Li et al [15] and Yang et al [12].

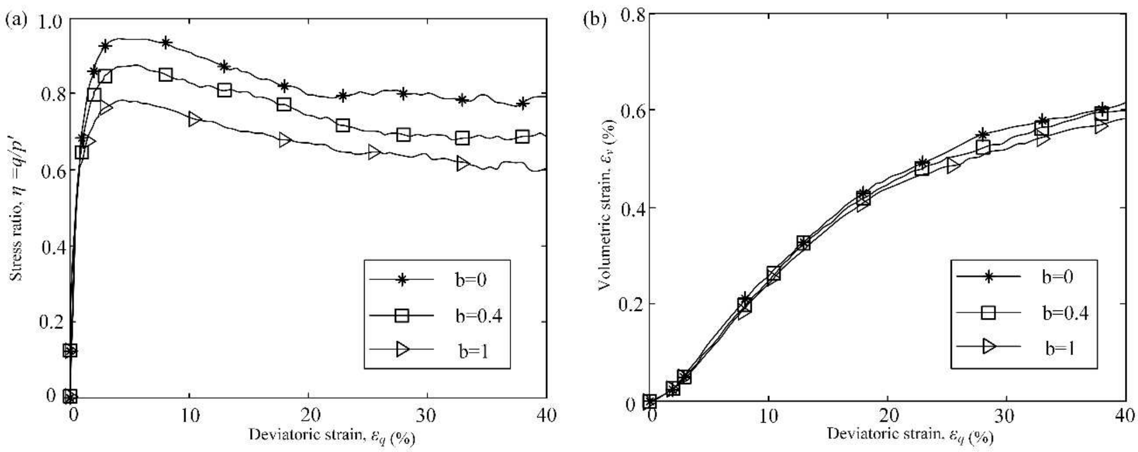

Fig.6 DEM simulation results on the effects of b-value on the response of stress-strain relations and volume change behaviours

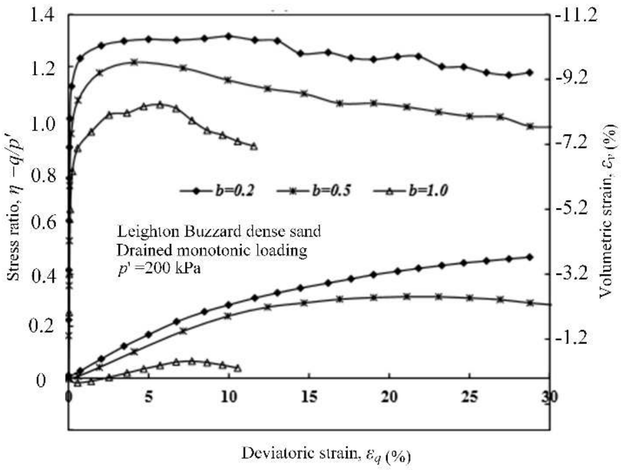

Fig.7 Hollow Cylinder experimental results on the effects of b-value on the response of stress-strain relations and volume change behaviours ([12])

3.12 Evolution of fabric deviator against the stress ratio

Fig.8 presents the evolution of the fabric deviator against the stress ratio for both DEM simulation results and theoretical results predicted by equation (2) and equation (7), in terms of dense specimens. Note that equation (2) is recovered from equation (7) by designating that $l_2 = l_1, l_3 = 1$. It can be clearly seen from the DEM results that the evolution of the fabric deviator for different b-values follows a similar pattern. The fabric deviator increases with the stress ratio at the initial stage of shearing until the stress ratio peaks. After that, the fabric deviator also achieves the peak value with a slight lag. The fabric deviator begins to decrease as the decreasing stress ratio continues to reach the critical value.

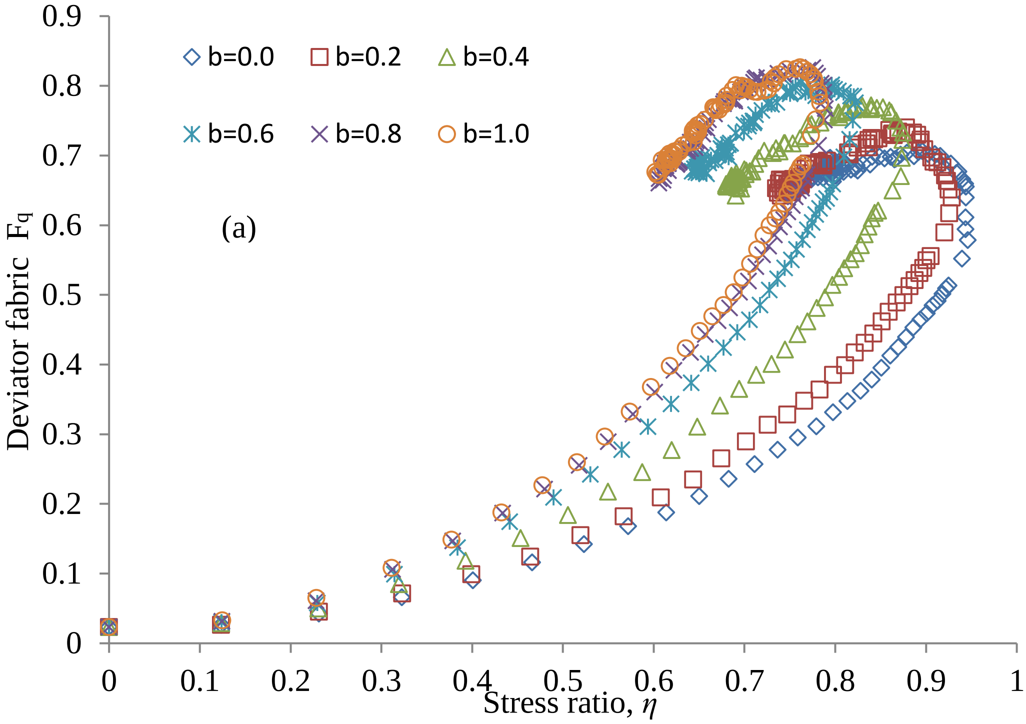
0.9
0.8
0.7
0.6
0.5
0.4
0.3
0.2
0.1
0
Deviator fabric Fq
b=0.0
b=0.2
b=0.4
b=0.6
b=0.8
b=1.0
(a)
0
0.1
0.2
0.3
0.4
0.5
0.6
0.7
0.8
0.9
1
Stress ratio, η

335

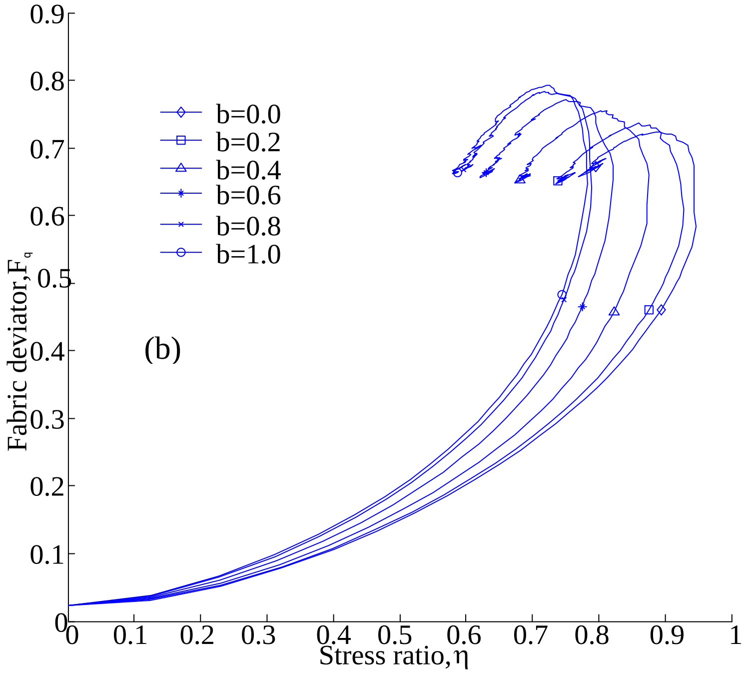
0.9
0.8
0.7
0.6
0.5
0.4
0.3
0.2
0.1
0
Fabric deviator,Fq
b=0.0
b=0.2
b=0.4
b=0.6
b=0.8
b=1.0
(b)
0
0.1
0.2
0.3
0.4
0.5
0.6
0.7
0.8
0.9
1
Stress ratio,η

336

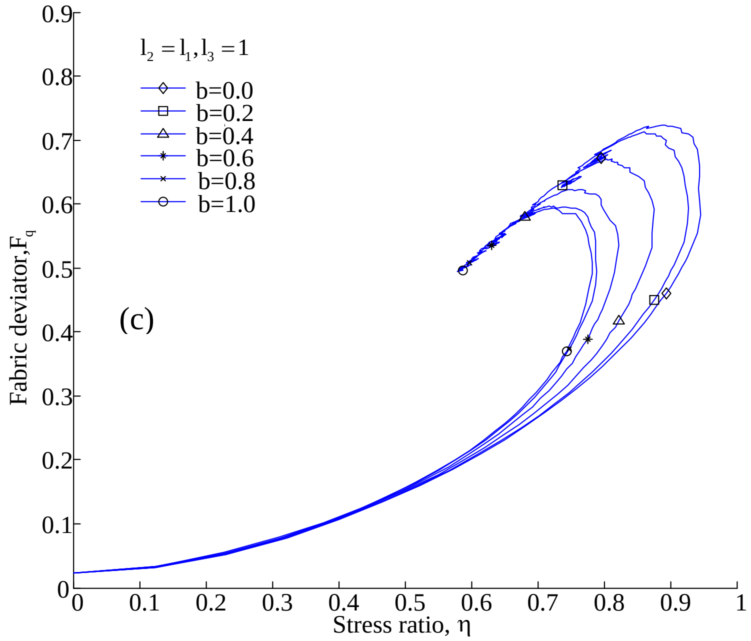

Fig. 8 The fabric evolution under proportional loading (dense sample): stress ratio η vs fabric deviator Fq: a) DEM simulation results; b) theoretical results from equation (7); c) theoretical results from equation (2).

The micromechanical interpretation of this phenomenon can be given through the stress-force-fabric (SSF) relationship proposed by Quadfel and Rothenburg [21]. In their study, the stress ratio was linearly related to the anisotropy degrees for contact normal density (i.e., fabric deviator) and the rest (e.g., normal contact force, tangential contact force, particle shape). The fabric deviator would follow the stress ratio to increase to a peak value. However, the anisotropy degrees for the rest would as well contribute to the stress ratio. According to the fabric evolution mechanism, the fabric deviator would exhibit a slag before approaching the peak value, and then decreased with the decreasing of the stress ratio to achieve a critical state. Yang [50] has analysed the evolution of contact normal by the DEM simulation results to explain this phenomenon. He presented that the vertical contact orientation is getting narrower, while the horizontal orientation is getting wider, with the increasing of shearing. The deviatoric stress ratio was increased since the sample was compressed. At the initial stage, the distribution of contact normal was homogeneous, demonstrating an isotropic state. The contact normal was continuously oriented to the vertical direction with the increasing of shearing. The fabric deviator was increasing until approaching a peak value. After that, the distribution of contact normal in the vertical direction was generally decreasing until reaching a critical state.

The b-value affects the peak and critical values of the fabric deviator; meanwhile, it affects the change of fabric deviator against the stress ratio. The peak fabric deviator increases with a greater b-value, while the peak stress ratio decreases with an increasing b-value, which is consistent with the observations by Thornton and Zhang [23] (Fig. 9). The evolution law in equation (7) can quantitatively capture the evolution of the fabric deviator.

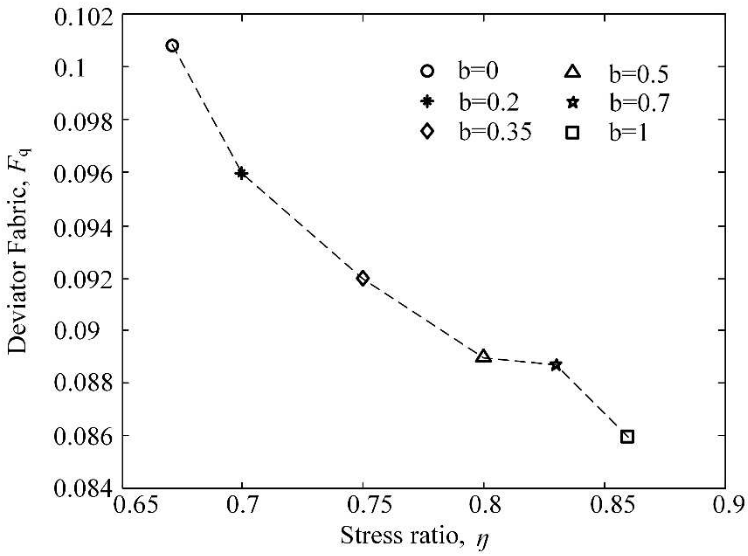

Fig.9 The peak stress ratio η vs fabric deviator Fq (Thornton and Zhang, 2010)

Fig.10 presents the evolution of the fabric deviator against the stress ratio for both DEM simulation results and theoretical results predicted by equation (7), in terms of loose specimens. Likewise, the evolution of the fabric deviator for different b-values follows a similar pattern. The fabric deviator increases with an increase in the stress ratio. The theoretical predictions shown in Fig. 10b can well capture the fabric deviator for a loose specimen. It should be noted that the present fabric evolution law is proposed by characterizing the influence of b-value on the critical state stress and critical state fabric; however, the critical state is not dependent on the initial void ratios (Yang [50]). Hence, comparisons between the DEM simulation results and theoretical predictions for both dense and loose samples demonstrate the applicability of the proposed evolution law to cases with various initial void ratios.

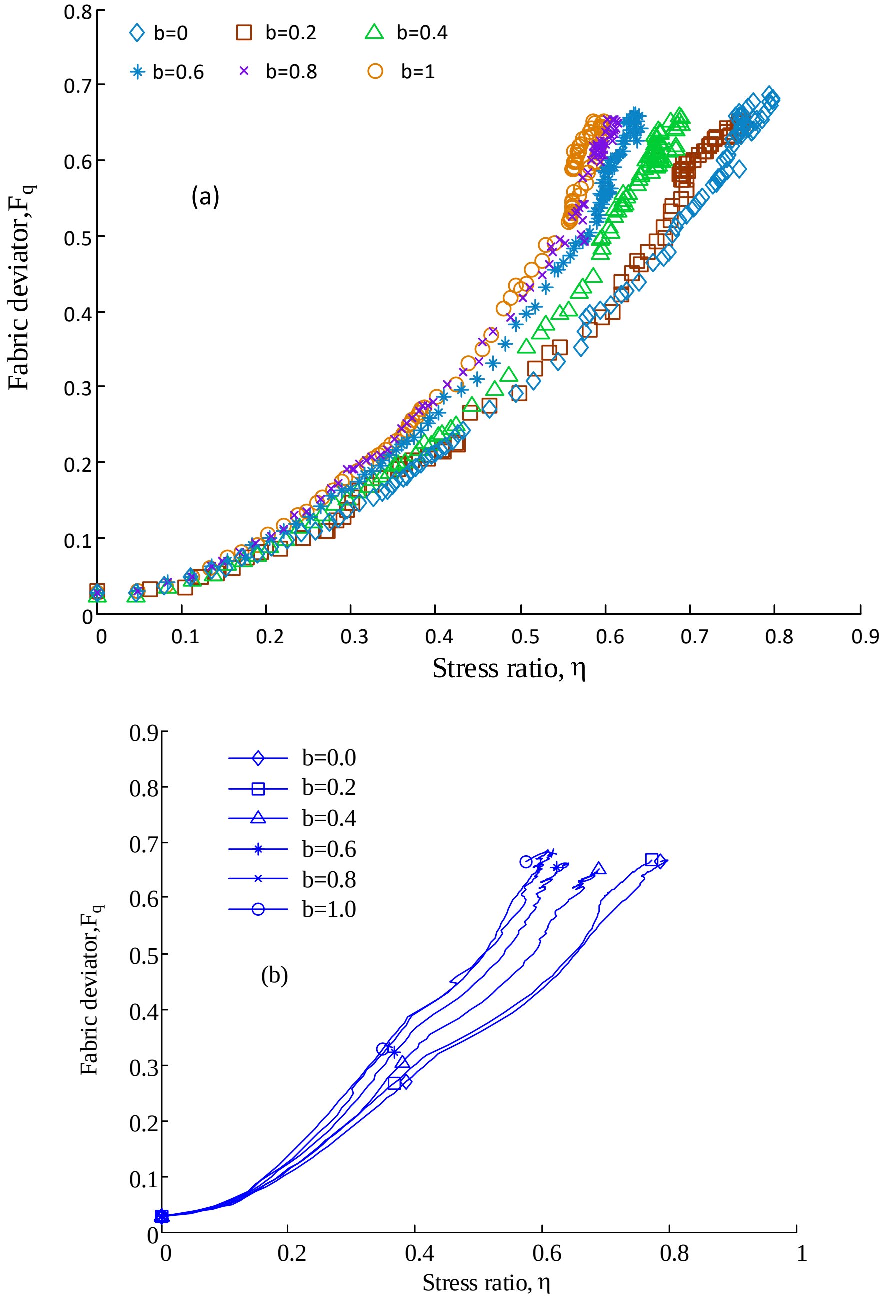

Fig.10 The fabric evolution under proportional loading (loose sample): stress ratio η vs fabric deviator Fq: a) DEM simulation results; b) theoretical results from equation (7)

3.13 Evolution of the intermediate fabric ratio against the stress ratio

Fig. 11 and Fig.12 present the evolution of the intermediate fabric ratio F_b ($F_b = (F_2 - F_3)/(F_1 - F_3)$) against the stress ratio for both DEM simulated results and theoretical predictions, corresponding to the dense and loose specimens, respectively. It can be seen from Fig. 11 and Fig. 12 that the evolution law in equation (7) can generally capture the effect of b-value on the evolution of F_b. For the dense specimen as shown in Fig. 11, in theoretical prediction, F_b reaches the b-value quickly before the peak stress ratio. In DEM results, even after the peak stress ratio, F_b still evolves towards the value of the intermediated stress ratio. In the fabric evolution law, it is assumed that the fabric tensor evolves towards the critical state and at the critical state F_b is the same as the b-value. With respect to the loose specimen as shown in Fig.12 a, F_b evolves towards the value of the intermediate stress ratio without a peak value. The theoretical predictions show that the fabric tensor evolves towards the critical state, where a larger final stress ratio is reached with a lower b-value. However as shown in both Fig. 11a and Fig. 12a, in DEM results, the final F_b is not exactly as the b-value, even it evolves towards b-value. This is because the real critical state is difficult to be achieved in DEM simulations due to the use of spheres in this study. The shear strain is not fully developed to give a critical state, since the shear strain is loaded to 40% in this study and the polyhedral shape used in our study can satisfactorily guarantee homogeneity of the sample [51]. Many researchers (e.g., [52]) have pointed out that critical states can only be reached at very large local shear deformations, e.g., the shear strain develops 70% or 100%, which are not always obtained by biaxial compression tests (both physical and numerical). Things would be different if non-spherical grains are used, which will be analysed in the future work.

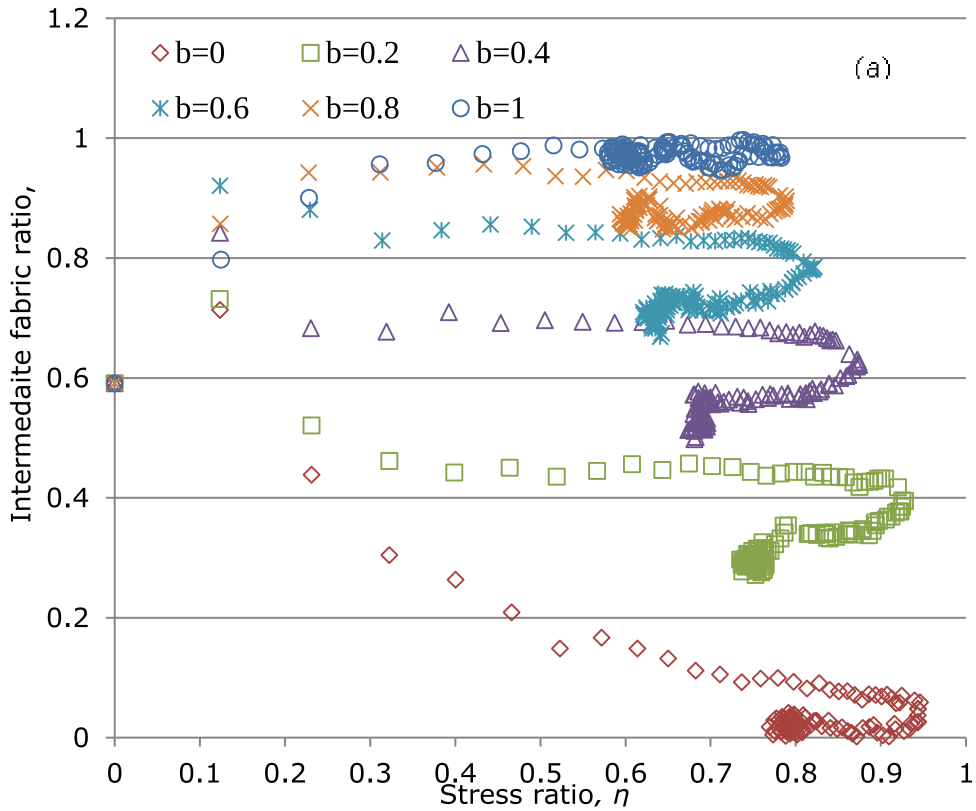

(a)
b=0
b=0.2
b=0.4
b=0.6
b=0.8
b=1
Intermedaite fabric ratio,
Stress ratio, η

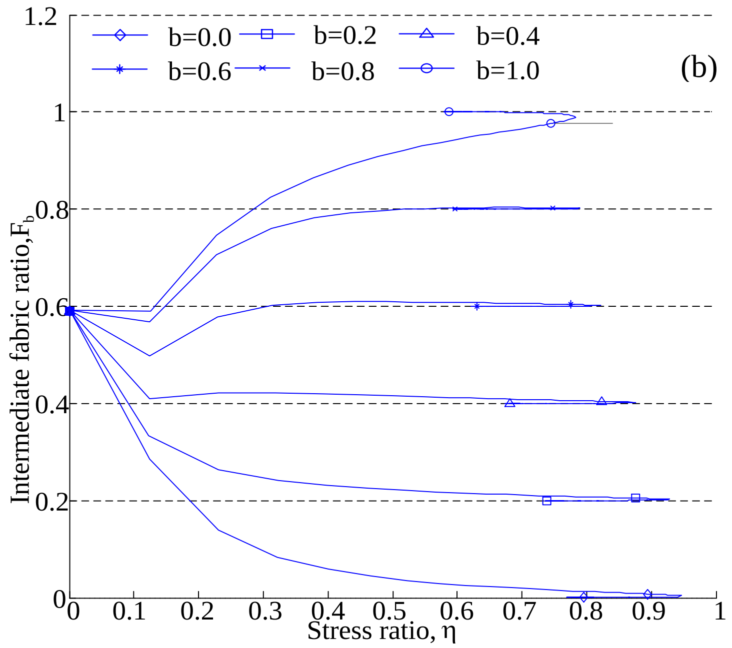

(b)
b=0.0
b=0.2
b=0.4
b=0.6
b=0.8
b=1.0
Intermediate fabric ratio,F_b
Stress ratio, η

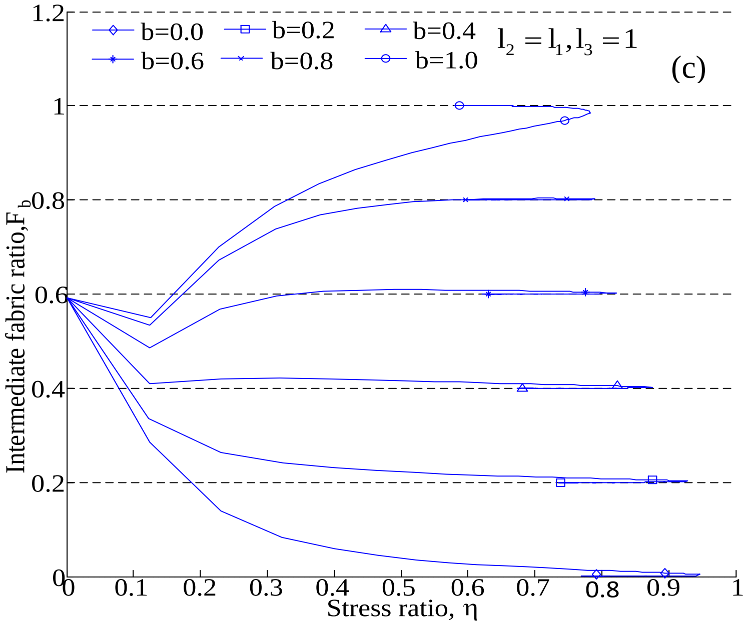

Fig. 11 The fabric evolution under proportional loading (dense sample): the stress ratio η vs the intermediate fabric ratio Fb: a) DEM simulation results; b) theoretical results from equation (7); c) theoretical results from equation (2).

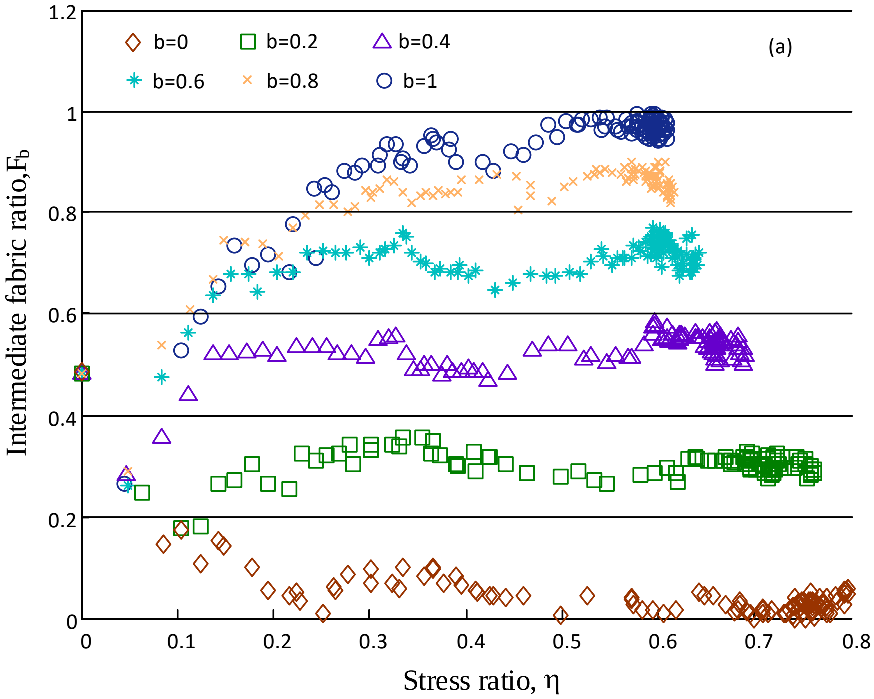

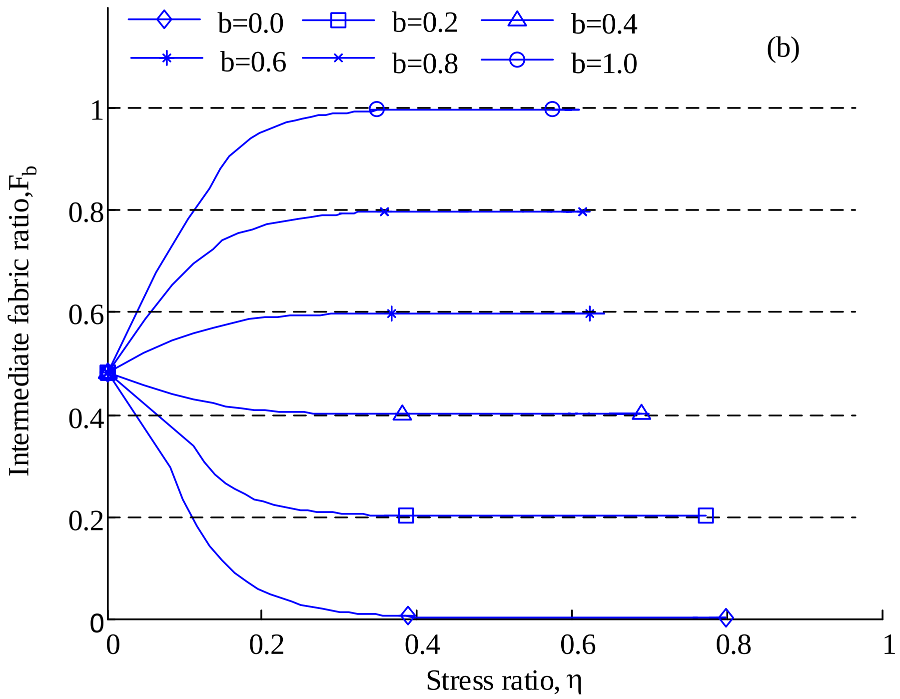

Fig. 12 The fabric evolution under proportional loading (loose sample): the stress ratio η vs the intermediate fabric ratio Fb: a) DEM simulation results; b) theoretical results from equation (7).

There is a large difference between the prediction and DEM results at a low stress ratio. This may be because the initial fabric of the sample used in DEM simulations is almost isotropic, i.e., the fabric deviator is very small. Hence the F_b is approximately singular. From this point of view, the DEM simulation results for F_b are meaningless at very small stress ratios because they cannot be accurately measured. The gap between the theoretical predictions and DEM simulation results, may be caused by the fact that the newly proposed evolution law is only concerned with two main mechanisms of the fabric evolution, i.e., the net rate of contact creation and migration of contact point, at a particle scale as shown in equation (7). Other secondary fabric evolution mechanisms, e.g., the convection and diffusion processes of contacts (due to that the contacts are continually created and broken during the deviatoric loading after the mitigation of contact points), are not taken into consideration. These secondary fabric mechanisms have been demonstrated not to be the main concern (e.g., [17, 51]).

Theoretical predictions by the evolution law in equation (2) are also presented in Fig.8c and Fig. 11c. In equation (2), C_F is taken as a constant independent of b-value. In a theoretical prediction, the integration stress-strain path is the true stress-strain path taken from DEM simulation results, and the critical stress ratio decreases with an increasing b-value. From equation (2.2), we can deduce that the predicted critical fabric anisotropy, determined by $M_F = C_F M$, also shows a similar trend as shown in Fig.8c. However, DEM results do not exhibit a similar trend. The predicted peak fabric anisotropy decreases with the increase in the b-value, which is obviously contradictory to the DEM results. The independency of C_F and C_1 from the b-value does not affect the predictions of F_b mainly because the initial fabric is almost isotropic and the increment of fabric tensor is proportional to the deviatoric stress tensor; hence, F_b approaches the intermediate stress ratio quickly in both predictions by both equations (2) and (7). When the initial fabric tensor is highly anisotropic, the approach of F_b to the intermediate stress ratio will be slower, and the performance of the fabric evolution law should be better, which can be shown by the results of the evolution of F_b in Hu [42].

From these comparisons, the generalized evolution law in equation (7) captures the effects of b-value on the fabric evolution well and greatly improves the performance of the evolution law in equation (2) in terms of the fabric deviator.

3.2 Parametric analysis

In the following computations, the shape parameters l_1 and l_2 are assumed to be the same as those used in the section 3.1. In all cases, the intermediate fabric ratio Fb and the principal directions of the fabric tensor quickly approach the stress tensor; hence, in the following analysis, only the results of the fabric deviator are presented in terms of the dense sample. The dense sample is taken as an example for simplicity since the following parameters are not obviously affected by the initial void ratio.

3.2.1 Parameter C_1 and shape parameter l_3

By comparing Fig. 13a with Fig. 13b, the effects of shape parameters l_3 on the first evolution mechanism related to the stress ratio tensor can be seen. As noted before, the first fabric evolution mechanism dominates the fabric evolution at a low stress ratio, because the plastic strain is negligible at this stage. When $l_3 = 1$, the shape function h_3 becomes independent of the b-value, and the predicted fabric deviators for different b-values coincide for the same C_1. However, when $l_3 = 1/l_1 > 1$, the shape function h_3 is an increasing function with a greater b-value, and fabric deviators increase quicker for a larger b-value. From both Fig. 13a and Fig. 13b, we can see that the rate of the fabric deviator increases with increasing C_1. Fig. 13c and Fig. 13d present the effects of the parameter C_1 and shape parameter l_3 on the evolution law. From Fig. 13c, we can see that because the second fabric evolution mechanism is also involved, the influence of l_3 on the fabric evolution decays with an increase in the stress ratio; after the peak stress ratio, the effects almost totally disappear. It can be seen in Fig. 13c that C_1 has a strong effect on the evolution of F_q up to the peak fabric deviator. However, after the peak stress ratio, the influence disappears gradually until the critical stress ratio. Because parameters C_1 and l_3 affect the fabric evolution through the first mechanism, their influences disappear when the influence of the first mechanism diminishes after the peak stress ratio.

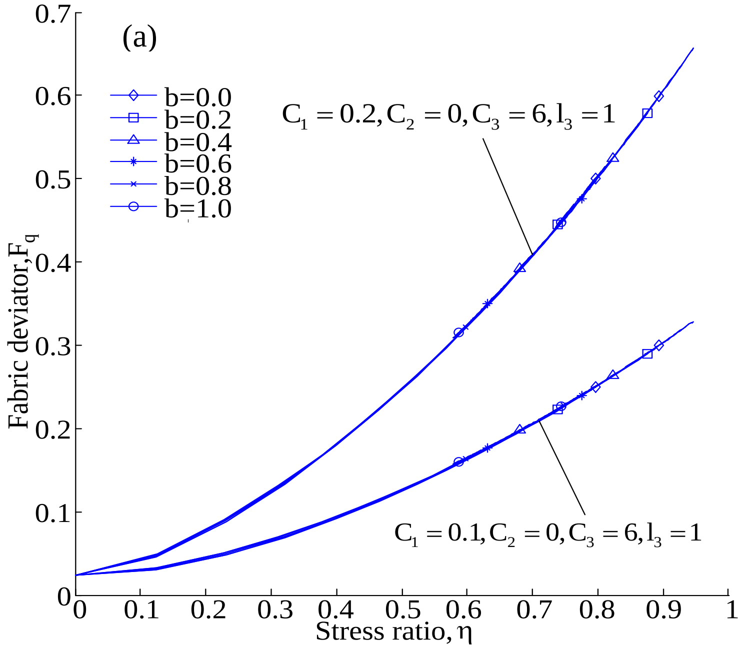
(a)
b=0.0
b=0.2
b=0.4
b=0.6
b=0.8
b=1.0
C1 = 0.2, C2 = 0, C3 = 6, l3 = 1
C1 = 0.1, C2 = 0, C3 = 6, l3 = 1
Fabric deviator, Fq
Stress ratio, η
0
0.1
0.2
0.3
0.4
0.5
0.6
0.7
0.8
0.9
1

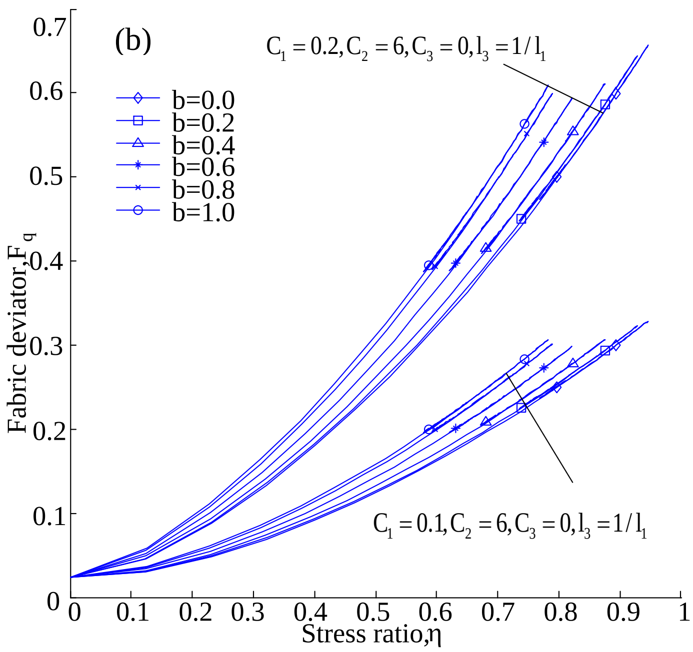
(b)
b=0.0
b=0.2
b=0.4
b=0.6
b=0.8
b=1.0
C1 = 0.2, C2 = 6, C3 = 0, l3 = 1/l1
C1 = 0.1, C2 = 6, C3 = 0, l3 = 1/l1
Fabric deviator, Fq
Stress ratio, η
0
0.1
0.2
0.3
0.4
0.5
0.6
0.7
0.8
0.9
1

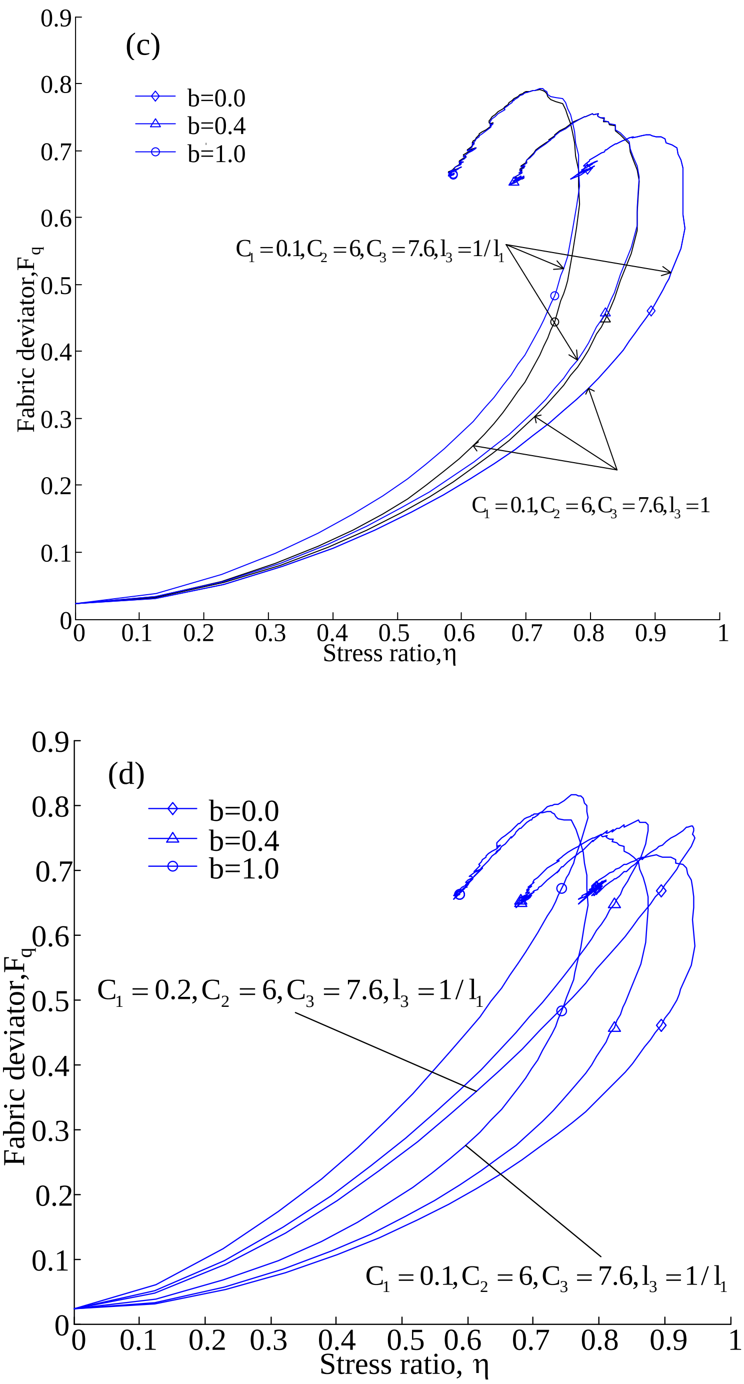

Fig. 13 Influences of C_1 and l_2 on the fabric deviator evolution

3.2.2 Parameter C_2

Parameter C_2 also affects the fabric evolution through the first evolution mechanism. In Fig. 14a, when the second mechanism is not involved, we can see that C_2 mainly affects the rate of increase of the fabric deviatoric against the stress ratio. When $C_2 = 0$, the relationship between

Fq and η becomes approximately linear. When $C_2 \neq 0$, the relationship is approximately quadric. For some case when simplicity is the primary concern rather than the accuracy, we can simply set $C_2 = 0$ together with another choice of C_1 to replace a more accurate set of C_1 and C_2. Fig. 14b again shows that the effects of C_2 last until the peak stress ratio, after which the effect of C_2 disappears.

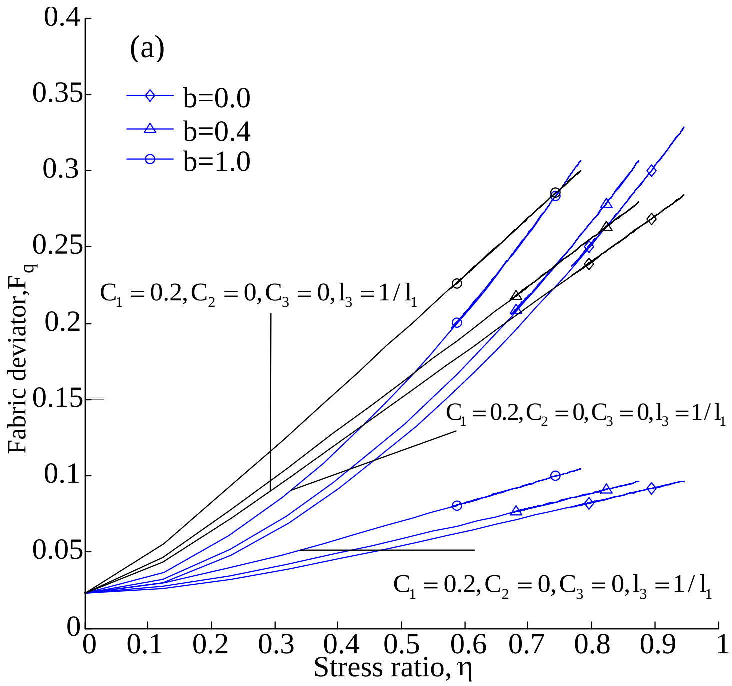

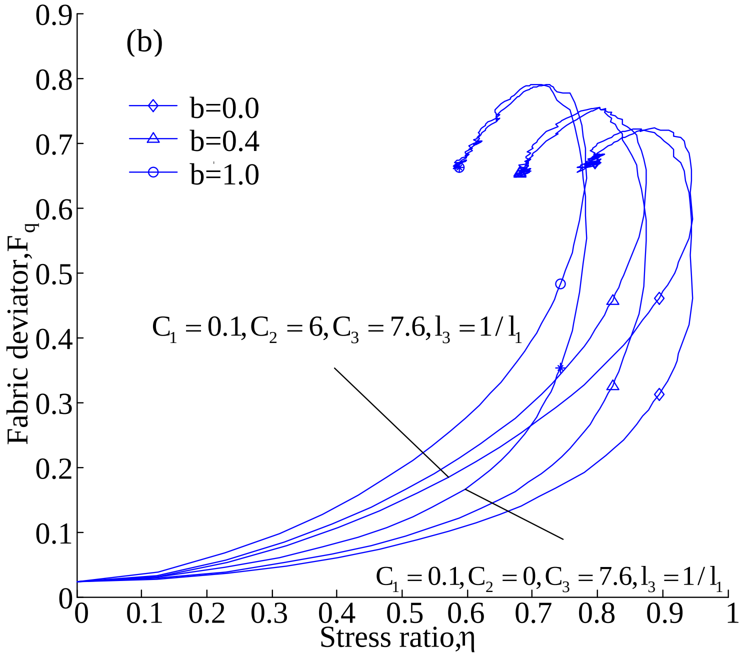

Fig. 14 Influences of C_2 on the fabric deviator evolution

3.2.3 Parameter C_3

Parameter C_3 affects the fabric evolution through the second evolution mechanism related to the plastic stress rate. The second mechanism ensures that the fabric evolves towards the critical fabric. In Fig.15 a, when the first mechanism is not involved, we can see that C_3 increases the

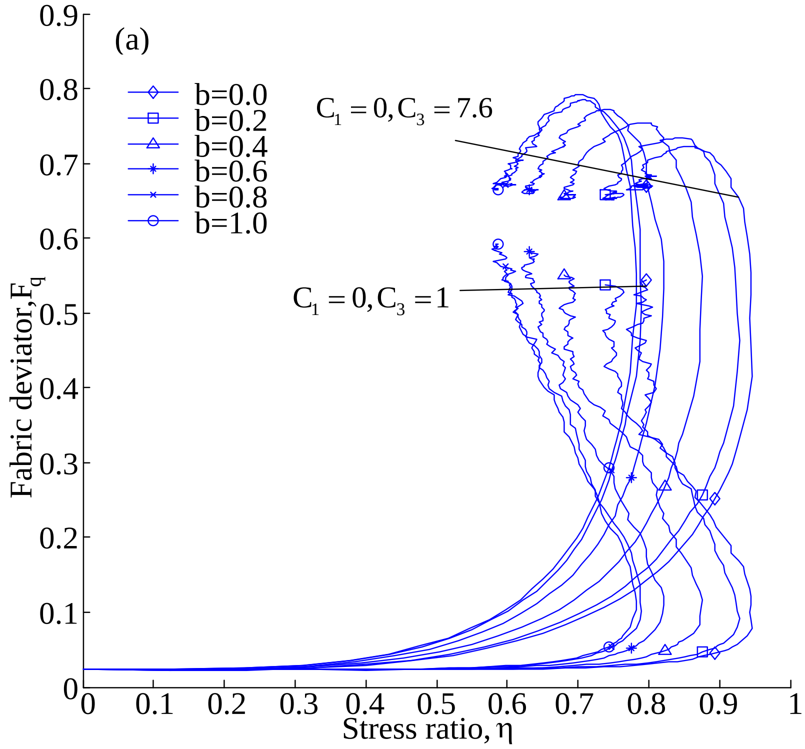

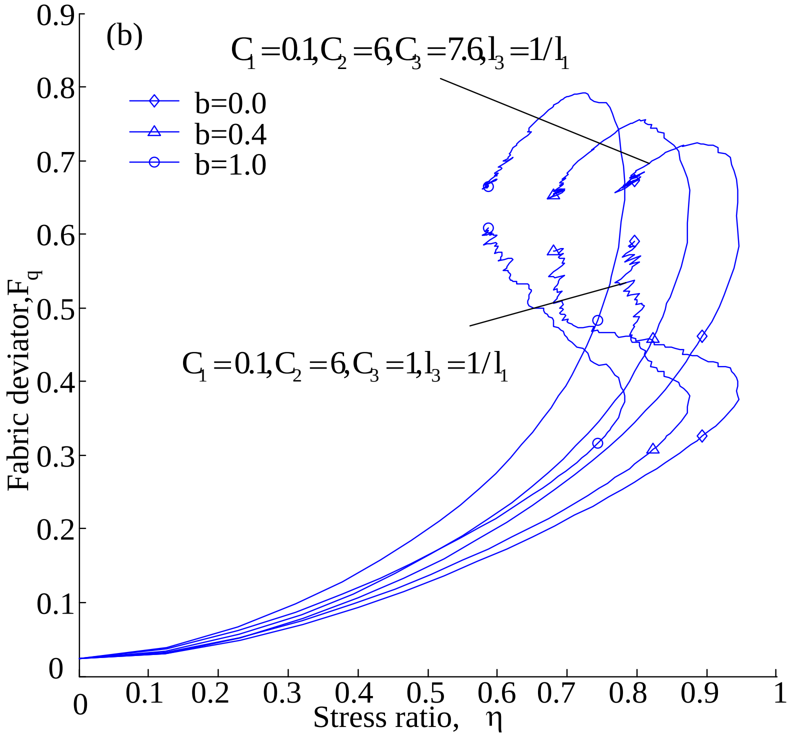

Fig. 15 Influences of C_3 on the fabric deviator evolution

rate of the fabric deviator towards the critical fabric deviator. When C_3 is smaller, the fabric evolves slower. C_3 does not have obvious effects on the fabric evolution at a low stress ratio; the influence of C_3 increases with an increasing stress ratio. If C_3 is not large enough, the evolution law may not predict a peak fabric deviator. When the first evolution mechanism is involved, as shown in Fig. 15 b, similar effects of C_3 on the fabric evolution can be observed.

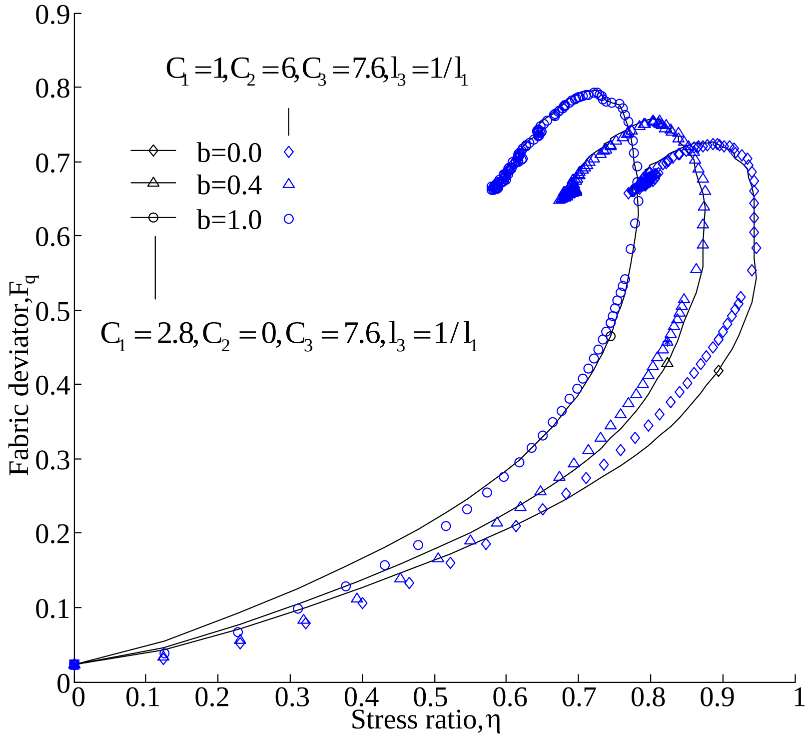

Fig. 16 Influences of the assumption $C_2 = 0, l_3 = 1/l_1$ on fabric deviator evolution

3.2.4 Discussion

From the parametric analysis, parameters C_1, C_2, l_3 affect the fabric evolution from the first mechanism, which dominates the fabric evolution at a low stress ratio. Parameter C_3 affects the fabric evolution from the second mechanism, which dominates the fabric evolution after the peak stress ratio when considerable plastic strain occurs. From this feature, we can determine the parameter C_3 by fitting curves of the stress ratio vs the fabric deviator after the peak stress ratio for a specific b-value, e.g., triaxial compression, and determine the parameters C_1, C_2, l_3 by fitting the curves of the stress ratio fabric deviator at a low stress ratio for a specific b-value. Because the influences of C_2, l_3 decay quickly due to the existence of the second evolution mechanism, we can simply assume that $C_2 = 0, l_3 = 1/l_1$ if the data are not available. Under this assumption, only parameter C_1 is left for determination. When the fabric evolution law is used for constitutive modelling considering the effects of initial and induced anisotropy and b-value, the assumption $C_2 = 0, l_3 = 1/l_1$ can reduce the amount of material parameters. Fig.16

presents the fabric deviator against the stress ratio for this assumption. From Fig.16, we can see that this assumption only affects the predicted accuracy at a very low stress ratio.

4 Concluding remarks

In this paper, the effects of b-value on the contact normal-based fabric evolution of granular materials were incorporated into an extant hybrid fabric evolution law. This new fabric evolution had the feature of material-frame indifference, rate-independency and uniqueness of critical state. The new fabric evolution law was validated by DEM simulation results with various initial void ratios. Conclusions can be drawn as follows:

- The new fabric evolution can capture the effects of b-value on the fabric evolution well for various initial void ratios, especially for the evolution of fabric deviator F_q. There was a gap between the theoretical predictions and DEM simulation results for F_b, due to the fact that only two main mechanisms, i.e., the net rate of contact creation and migration of contact point, of the fabric evolution were concerned in the present fabric evolution law.
- Parametric study was carried out to analyse the influences of parameters C_1, C_2, C_3, l_3. For simplicity, the setting of parameters for the fabric evolution law in equation (7) can be reduced to 5 independent parameters, i.e., $(C_1, C_3, M, M_{Fc}, M_{Ft})$.
- The proposed evolution law can act as a fundamental aid for further development of fabric constitutive modelling of granular materials, accounting for the effects of b-value and material anisotropy, combined with simple isotropic constitutive models (e.g., the CASM Model).

In this paper, we limited the stress path in the monotonic loading with a fixed loading direction. The evolution law has not been validated to consider the b-value on fabric evolution for more complicated stress path, e.g., pure rotational shearing, which needs further investigation.

5 Acknowledgement

This work was supported by the National Natural Science Foundation of China (Grant No.51609204, 51608454) and the Fundamental Research Funds for the Central Universities (Grant No. 2682015CX092, 2682016CX084). In addition, the authors would like to thank Prof. Xia Li, School of Civil Engineering in Southeast University, for her valuable guidance and support to this work.

References

[1] Habib P. Influence de la variation de la contrainte principale moyenne sur la résistance au cisaillement des sols. Proceedings of the 3rd International Conference on Soil Mechanics and Foundation Engineering 1953;131-136.

[2] Bishop AW. The Strength of Soils as Engineering Materials. Géotechnique 1966;16(2):91-130.

[3] Bjerrum L, Kummeneje O. Shearing resistance of sand samples with circular and rectangular cross sections. NGI Report, NR 1961;44(1-7).

[4] Cornforth DH. Some experiments on the influence of strain conditions on the strength of sand. Géotechnique 1964;14(2):143-167.

[5] Oda M, Koishikawa I, Higuchi T. Experimental study of anisotropic shear strength of sand by plane strain test. Soils and foundations 1978;18(1):25-38.

[6] Lade PV, Duncan J M. Cubical Triaxial Tests on Cohesionless Soil. Journal of the Soil Mechanics and Foundations Division 1973;99(10):793-812.

[7] Arthur JRF, Chua KS, Dunstan T. Induced anisotropy in a sand. Géotechnique 1977;27(1):13-30.

[8] Nabil, SE. Shear strength of a cohesionless soil under plane strain and triaxial conditions. , Open Access Dissertations and Theses. Paper 484; 1976.

[9] Symes MJ. Rotation of principal stresses in sand. PhD Thesis, Imperial College of Science, Technology and Medicine, University of London, 1983.

[10] Sayao ASFJ, Vaid YP. Effect of intermediate principal stress on the deformation response of sand. Canadian Geotechnical Journal 1996;33(5):822-828.

[11] Yoshimine M, Ishihara K, Vargas W. Effects of principal stress direction and intermediate principal stress on undrained shear behavior of sand. Soils and Foundations 1998;38(3):179-188.

[12] Yang, L.T. Li, X. Yu, H.S. Wanatowski, D. A laboratory study of anisotropic geomaterials incorporating recent micromechanical understanding, Acta Geotechnica 2016; 11:1111.

[13] Thornton C. Numerical simulations of deviatoric shear deformation of granular media. Géotechnique 2000;50(1):43-53.

[14] Thornton C, Zhang L. A numerical examination of shear banding and simple shear non-coaxial flow rules. Philosophical Magazine 2006;86(21-22):3425-3452.

[15] Li X., Yang D.S., Yu. H-S. Macro deformation and micro structure of 3D granular assemblies subjected to rotation of principal stress axes, Granular Matter 2016, 18:53.

[16] Li B, Chen LL, Gutierrez M. Influence of the intermediate principal stress and principal stress direction on the mechanical behavior of cohesionless soils using the discrete element method. Computers and Geotechnics 2017;86:52-66.

[17] Kuhn MR. Micro-mechanics of fabric and failure in granular materials. Mechanics of Materials 2010;42(9):827-840.

[18] O'sullivan C, Wadee MA, Hanley KJ, Barreto D. Use of DEM and elastic stability analysis to explain the influence of the intermediate principal stress on shear strength. Géotechnique 2013;63(15):1298-1309.

[19] Kanatani KI. Distribution of directional data and fabric tensors. International Journal of Engineering Science 1984;22(2):149-164.

[20] Li X, Yu HS, Li XS. Macro–micro relations in granular mechanics. International Journal of Solids and Structures 2009;46(25):4331-4341.

[21] Ouadfel H, Rothenburg L. 'Stress–force–fabric' relationship for assemblies of ellipsoids. Mechanics of materials 2001;33(4):201-221.

[22] Li X, Yu HS. On the stress–force–fabric relationship for granular materials. International Journal of Solids and Structures 2013;50(9):1285-1302.

[23] Thornton C, Zhang L. On the evolution of stress and microstructure during general 3D deviatoric straining of granular media. Géotechnique 2010;60(5):333-341.

[24] Zhao J, Guo N. Unique critical state characteristics in granular media considering fabric anisotropy. Géotechnique 2013a;63(8):695-704.

[25] Matsuoka H, Nakai T. Stress-deformation and strength characteristics of soil under three different principal stresses. Proceedings of the Japan Society of Civil Engineers: Japan Society of Civil Engineers, 1974. 232:59-70.

[26] Lade PV, Duncan JM. Elastoplastic Stress-Strain Theory for Cohesionless Soil. Journal of the Geotechnical Engineering Division 1975;101(10):1037-1053.

[27] Lade PV. Failure criterion for cross-anisotropic soils. Journal of geotechnical and geoenvironmental engineering 2008;134(1):117-124.

[28] Sheng D, Sloan SW, Yu HS. Aspects of finite element implementation of critical state models. Computational mechanics 2000;26(2):185-196.

[29] Ma C, Lu D, Du XL, Zhou AN. Developing a 3D elastoplastic constitutive model for soils: A new approach based on characteristic stress. Computers and Geotechnics 2017;86:129-140.

[30] Gao ZW, Zhao JD, Li XS, Dafalias YF. A critical state sand plasticity model accounting for fabric evolution. International journal for numerical and analytical methods in geomechanics 2014;38(4):370-390.

[31] Xiong H, Nicot F, Yin ZY. A three‐dimensional micromechanically based model. International Journal for Numerical and Analytical Methods in Geomechanics 2017.

[32] Yu HS. CASM: A unified state parameter model for clay and sand. International Journal for Numerical and Analytical Methods in Geomechanics 1998;22(8):621-653.

[33] Yu HS. Plasticity and geotechnics: Springer Science & Business Media; 2007.

[34] Rothenburg, L., Bathurst, R.J. Analytical study of induced anisotropy in idealized granular materials. Géotechnique 1989; 39 (4). 601-614.

[35] Sitharam TG, Vinod JS, Ravishankar BV. Post-liquefaction undrained monotonic behaviour of sands: experiments and DEM simulations. Géotechnique 2009; 59(9):739–49.

[36] Guo N, Zhao J.D. The signature of shear-induced anisotropy in granular media. Computer and Geotechnics 2013; 47:1-15.

[37] Yu, H.-S. Non-coaxial theories of plasticity for granular materials. The 12th International Conference of International Association for Computer Methods and Advances in Geomechanics. Goa, India 2008.

[38] Schofield, A. and C. P. Wroth. Critical State Soil Mechanics. London, McGraw-Hill 1968.

[39] Been, K., et al. The critical state of sands. Géotechnique 1991; 41(3): 365-381.

[40] Wood, D. M. Soil behaviour and critical state soil mechanics. Cambrige University Press 1991.

[41] Ishihara, K. Liquefaction and flow failure during earthquakes. Géotechnique 1993; 43(3): 351-451.

[42] Hu N. On Fabric Tensor-based Constitutive Modelling of Granular Materials: Theory and Numerical Implementation. PhD Thesis, University of Nottingham, 2015.

[43] Loukidis D, Salgado R. Modeling sand response using two-surface plasticity. Computers and Geotechnics 2009;36(1):166-186.

[44] Itasca Consulting Group Inc.: PFC2D (Particle Flow Code in TwoDimensions). In. ICG, Minneapolis, 1999.

[45] Haruyama, M. Anisotropic deformation-strength characteristics of an assembly of spherical particles under three dimensional stresses. Soils and Foundations 1981; 21, 41-55.

[46] LADE, P. V. & ABELEV, A. V. Characterization of cross-anisotropic soil deposits from isotropic compression tests. Soils and Foundations 2005; 45, 89-102.

[47] Li, X., H-S, Yu., X-S Li. A virtual experiment technique on the elementary behaviour of granular materials with discrete element method. International Journal for Numerical and Analytical Methods in Geomechanics 2013; 37: 75-96.

[48] Li, X., et al. Macro-micro relations in granular materials. International Journal of Solids and Structures 2009; 46: 4331-4341.

[49] OCHIAI, H. & LADE, P. V. Three-dimensional behaviour of sand with anisotropic fabric. Journal of Geotechnical Engineering 1983; 109, 1313-1328.

[50] Yang D.S. Microscopic Study of Granular Material Behaviours under General Stress Paths. PhD Thesis, University of Nottingham, 2014.

[51] Ma, X., Zhang, D.Z. Statistics of particle interaction in dense granular material under uniaxial compression. J. Mech. Phys. Solids 2006; 54, 1426–1448.

[52] Fu, P. and Y. F. Dafalias (2011). "Fabric evolution within shear bands of granular materials and its relation to critical state theory." International Journal for Numerical and Analytical Methods in Geomechanics 35(18): 1918-1948.